State-Dependent Dilatancy of Soils: Experimental Evidence and Constitutive Modeling

Merita Tafili[1(✉)] and Theodoros Triantafyllidis[2]

[1] Institute of Soil Mechanics and Rock Mechanics (IBF), Karlsruhe, Germany
merita.tafili@kit.edu
[2] IBF, Karlsruhe, Germany
theodoros.triantafyllidis@kit.edu

Abstract. This work provides a new evaluation method of the *dilatancy* for cohesive soils from monotonic and cyclic undrained triaxial tests. Herein it is implemented for experiments performed on Kaolin. Leastwise for this soft soil the *dilatancy* turns out to be a function of the stress ratio η and the void ratio e along with the intrinsic material parameters. Furthermore, an OCR-definition, which includes the influence of both the stress ratio and void ratio such that $d = f(\mathrm{OCR}, C)$ with C being a set of inherent parameters is proposed. In addition based on the experimental observations it is suggested that there is an overconsolidation ratio OCR_{ci} at which the soft soil behaviour changes from contractant in case of $\mathrm{OCR} < \mathrm{OCR}_{ci}$ to dilatant (the material can both contract and dilate depending on η) in case of $\mathrm{OCR} > \mathrm{OCR}_{ci}$ with the PTL lying below the CSL in this case. Finally, a constitutive relation describing the behaviour of soft soils including the *dilatancy* and viscosity is proposed. Some simulations of monotonic as well as cyclic tests are shown to prove the accurate performance of the model.

1 Introduction

The design of geotechnical installations in offshore constructions for example gravity platforms, piled installations, suction anchors, drilling rigs, wind turbines or constructions along the coast for example harbours, breakwaters, dams, storm-surge barriers is governed by the bearing capacity and the serviceability of the structures under cyclic loading [1]. In most of these cases, the underground consists of soft and normalconsolidated clays, sand-clay or sand-silt mixtures. A soft normalconsolidated clay subjected to cyclic loading passes through different overconsolidation ratios $\mathrm{OCR} \geq 1$. Though if the cyclic behaviour of a normalconsolidated clay with a moderately number of cycles is described, the behaviour of an overconsolidated clay is captured by the way. Various effects of clays become increasingly important at different stages of these cyclic tests as for example at the beginning $\mathrm{OCR} = 1$ the time-dependent behaviour of a plastic clay achieves its maximum. For $1 < \mathrm{OCR} \leq 2$ the rate-dependency of

T. Triantafyllidis (Ed.): *Recent Developments of Soil Mechanics and Geotechnics in Theory and Practice*, LNACM 91, pp. 54–84, 2020.
https://doi.org/10.1007/978-3-030-28516-6_4

the clay decays sparsely and depending on the subjected loading magnitude the response of the material is contractant. This leads to the generation of excess pore water pressure resulting in a reduction of the bearing capacity and decay of the barotropic soil stiffness. Towards higher OCR > 2 a significant reduction of the viscous effects is evident, whereby now the materials' phase transformation line (PTL) lies below the critical state line, thus besides contractancy also dilatant behaviour can be observed when reaching the PTL.

Dilatancy and contractancy, hereafter referred to collectively as *dilatancy*, are highly relevant for geotechnical issues dealing with volumetric change due to shearing. Under undrained conditions the prevented dilatancy leads to an increase of the mean pressure and the prevented contractancy can lead to a considerable decay of the same pressure. The consequences are then an increasing accumulation of the pore water preassure, a decay of the barotropic stiffness as well as a considerable reduction of the shear strength q_{max}. Accurate and reliable predictions of post-seismic irreversible displacements in retaining structures supporting fine-grained and low-permeable soils can therefore be obtained only if the adopted constitutive model is capable of capturing correctly the soil *dilatancy* as a function of the current stress and loading history [2]. Furthermore, the *dilatancy* is shown to depend also on other state variables as the void ratio e [3–8] as well as on the sample preparation method [9].

The *dilatancy* of sands has been the research target of many authors [3–8] in the last decades. Among others, Taylor documented in [3]: "The shearing strength" $\tau_m = \sigma \tan \varphi_m$ "in sand may be said to consist of two parts, the internal, frictional resistance between grains, which is a combination of rolling and sliding friction," $\tau_c = \sigma \tan \varphi_c$ "and a second factor for which the most common name is *interlocking*." $\tau_d = \sigma \tan \varphi_d = \sigma \tan \psi$. "Interlocking contributes a large portion of the strength in dense sands; this phenomenon does not occur in very loose sands. The gradual loss of strength after the peak point is passed, ..., may be attributed to a gradual descrease in interlocking which takes place because the sample is decreasing in density. The angle of internal friction, in spite of its name, does not depend solely on internal friction, since a portion of the shearing stress on a plane of failure is utilized in overcoming interlocking."[1] which mathematically can be expressed through:

$$\tau_m = \tau_c + \tau_d \tag{1}$$

whereby the subscripts m, c and d denote the mobilized, critical and *dilatant* state, respectively. Further Taylor [3] suggests: "Interlocking can best be explained by considerations of strain energy. Sands generally are undergoing increase in volume" (expansion) "when the ϕ-obliquity condition is reached," $E_e^d = \sigma A \Delta h$ (superscript d stays for dissipated, subscript e stays for expansion) "and the part of the shearing stress that is acting to overcome interlocking may also be said to be supplying the energy that is being expended in volume increase." (See footnote 1) $E_e^s = \tau A \Delta u$ (superscript s stays for supplied). Assuming $\sigma = const.$ as defined in Fig. 1 we can establish the equilibrium between these two energies:

[1] Taylor in 1954 [3], pp. 345–347.

$$E_e^d = E_e^s \Rightarrow \sigma A \Delta h = \tau A \Delta u \Rightarrow \tau = \sigma \Delta h / \Delta u \tag{2}$$

Due to the equality between the shear strength during expansion τ with the shear strength resulting from interlocking τ_d, Eq. 1 can be rewritten to:

$$\sigma \tan \varphi_m = \sigma \tan \varphi_c + \sigma \Delta h / \Delta u \tag{3}$$

$$\Rightarrow \quad \tan \varphi_m = \tan \varphi_c + \tan \psi. \tag{4}$$

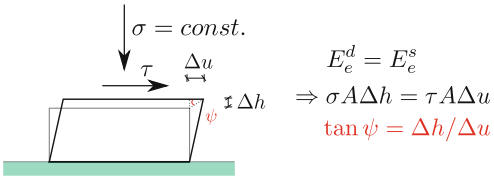

Fig. 1. Shearing of a dense sand with interlocking.

Note that the assumption $\sigma = const.$ guarantees that the volume change dv_d is induced by pure shearing. Otherwise, for example in an undrained or drained triaxial test ($p \neq const.$) the knowledge about the elasticity of the material is required in order to identify which portion of the volumetric and shear change is due to the variation of the applied stresses and which one due to interlocking. In this case instead of the normal σ and shear τ stresses, the stress tensor $\boldsymbol{\sigma}$ is used and instead of the height change Δh and the horizontal displacement Δu, the strain tensor $\boldsymbol{\varepsilon}$ is used. Then, the *dilatancy* is expressed through the ratio between the increment of the plastic volumetric change and the plastic shear strain increment:

$$d = dv^p / |d\gamma^p|. \tag{5}$$

Although the particular forms proposed by Taylor [3] and by Rowe [4] were different, both of them recommended a unique function dependent on the stress ratio $\eta = q/p$ for the *dilatancy*, as depicted by Li and Dafalias [6] $d = d(\eta, C)$ whereby C is a set of inherent material properties. However, experimental evidence postulates [5,9–11] a density dependence of the *dilatancy* as well. For example dense sand dilates after minor initial contractancy and loose sand contracts during shearing. For this purpose researchers proposed various expressions of state-dependent *dilatancy* for sands, which will be reviewed in Sect. 3 after the formal extension from direct shear to triaxial conditions, which are provided in Sect. 2.

On the other side, too little attention has been paid to the dilatant behaviour of clays. Li and Dafalias [6] indicate that $d = d(\eta, M)$ with the slope of the critical state line denoted as M works quite well for clays. This may correspond for normalconsolidated clays (compare the behaviour of loose sands). However, experimental evidence has shown that overconsolidated clays dilate [9,12–15] showing a similar response as medium dense and dense sand. Section 4 provides

an overview and the evaluation of experimental data on normal- and overconsolidated clays regarding their *dilatancy*. Then, in Sect. 5 a state dependent *dilatancy* for clays is formulated. Finally, the reference model [15] is extended to account for the *dilatancy* of clays. The models' performance is evaluated through simulations of experimental data of Kaolin with variation of initial OCR_0.

2 From Direct Shear to General Conditions

In a general case the material state is described through the stress tensor $\boldsymbol{\sigma}$ replacing the normal stress σ and the shear stress τ and through the strain rate (increment tensor) $\dot{\boldsymbol{\varepsilon}}$ ($d\boldsymbol{\varepsilon}$). The dilatancy is then defined as the negative ratio between the irreversible strain invariants: plastic volumetric strain increment and the plastic deviatoric strain increment:

$$d = -d\varepsilon_v^p / |d\varepsilon_q^p|. \tag{6}$$

In order to generalize the dilatancy rule given in Eq. 4 we start with the thermodynamic equilibrium of a direct shear test whereby the introduced power density $\tau\dot{\gamma} + \sigma\dot{\varepsilon}$ is partly stored as elastic power $\tau\dot{\gamma}^e + \sigma\dot{\varepsilon}^e$ and partly converted into heat due to the friction between the grain contacts $\tan\varphi_c\,\sigma|\dot{\gamma}^p|$. Thus, a constraint on the plastic strain rates (i.e. on the flow rule) can be established from the relation:

$$\tau\dot{\gamma}^p + \sigma\dot{\varepsilon}^p = \tan\varphi_c\sigma|\dot{\gamma}^p|. \tag{7}$$

Due to the vanishing plastic strains at reversals in elasto-plasticity, it is more convenient to rewrite Eq. 7 with total strain rates:

$$\tau\dot{\gamma} + \sigma\dot{\varepsilon} = \tan\varphi_c\sigma|\dot{\gamma}|. \tag{8}$$

Note that the relation 8 is deduced considering $\sigma = const$. For triaxial conditions Eq. 8 reads $q\dot{\varepsilon}_q + p\dot{\varepsilon}_v = M\,p\,|\dot{\varepsilon}_q|$ and using the energetically conjugated tensorial values $\boldsymbol{\sigma} : \dot{\boldsymbol{\varepsilon}}$ for the left hand side and $\dot{\boldsymbol{\varepsilon}}^*$ for the last therm on the right hand side the generalization of the *dilatancy* rule given in Eq. 8 is straightforward and reads:

$$\boldsymbol{\sigma} : \dot{\boldsymbol{\varepsilon}} = \sqrt{\frac{2}{3}}\frac{1}{3}M\,\mathbf{1} : \boldsymbol{\sigma}|\dot{\boldsymbol{\varepsilon}}^*| \tag{9}$$

with $p = \mathbf{1} : \boldsymbol{\sigma}/3 = const$. Relations 7, 8 and 9 operate as *dilatancy* constraints for both loading $\boldsymbol{\varepsilon}_q > 0$ and for unloading $\boldsymbol{\varepsilon}_q < 0$ conditions. In order to impose this constraint in an for example isotropic elastic model an anisotropic term E_{pq} of the stiffness tensor for the consideration of dilatancy is necessary. Without loss of generality we consider triaxial conditions:

$$\begin{bmatrix}\Delta p\\ \Delta q\end{bmatrix} = \begin{bmatrix}E_{pp} & E_{pq}\\ 0 & E_{qq}\end{bmatrix}\begin{bmatrix}\Delta\varepsilon_v\\ \Delta\varepsilon_q\end{bmatrix} \tag{10}$$

with $E_{pp} = K$ and $E_{qq} = 3G$. Imposing the *dilatancy* constraint according to Eq. 9 for $\Delta p = 0$ the coupling stiffness therm between the increment of p and of ε_q reads:

$$E_{pq} = E_{pp}\,(M - \eta). \tag{11}$$

Obviously, an undrained shearing $\dot{\varepsilon}_v = 0$ simulated with the model given in Eq. 10 produces contractancy resulting in mean pressure reduction $\Delta p < 0$. To impose the condition given in Eq. 9 in a sophisticated constitutive model is however almost impossible. For this reason the generalization of other variables that define the *dilatancy* is indispensable.

Pradhan and Tatsuoka reported in [10] the following two relations between the *dilatancy* d (herein defined in strain invariants, see Eq. 6) and the dilatancy angle ψ for isobaric triaxial conditions:

$$d = \begin{cases} \frac{3}{2}\frac{4\sin\psi}{3-\sin\psi} = \frac{6\sin\psi}{3-\sin\psi} & \text{for axial compression } (d\varepsilon_q > 0) \\ -\frac{3}{2}\frac{4\sin\psi}{3+\sin\psi} = -\frac{6\sin\psi}{3+\sin\psi} & \text{for axial extension } (d\varepsilon_q < 0). \end{cases} \tag{12}$$

Note that the factor 3/2 on the RHS is introduced because Pradhan & Tatsuoka used $d\gamma^p$ instead of the invariant $d\boldsymbol{\varepsilon}_q^p = 2/3\, d\gamma^p$ appearing in Eq. 6. Taking into consideration for example the Matsuoka-Nakai failure criterion [16] and the Mohr-Coulomb criterion as well, the slope of the critical state line in triaxial compression and triaxial extension with respect to the critical friction angle φ_c reads:

$$M = \begin{cases} \frac{6\sin\varphi_c}{3-\sin\varphi_c} & \text{for compression } (q > 0) \\ -\frac{6\sin\varphi_c}{3+\sin\varphi_c} & \text{for extension } (q < 0) \end{cases} \tag{13}$$

The analogy between d given in Eq. 12 and M presented in Eq. 13 is obvious. Yet, it is mandatory to realize the difference in the definition of compression and extension whether using the stress or the strain. The definition for the critical state (CS) is realised in the **stress space** with $q > 0$ for compression and $q < 0$ for extension. Thus, the generalization of M to multiaxial space is executed by means of the Lode angle of the **stress** $\theta_{\boldsymbol{\sigma}}$:

$$M = \frac{6\sin\varphi_c}{3-\sin\varphi_c\cos(3\theta_{\boldsymbol{\sigma}})} \tag{14}$$

A similar relation leading to same results was proposed by Argyris et al. [17] and was used for other constitutive models e.g. [18–20]. The link between the stress and the strain in CS is established through the critical void ratio, to be defined in Eq. 23.

Yet, when we consider the same stress ratio η (viz. same stress state), two different values for d depending on the direction of straining increment are possible as documented by Pradhan et al. [5] for sands (experiments from [5] are illustrated exemplarily in Fig. 3). Figure 2b shows two different stress states (but three strain states Fig. 2a, c) with different loading and straining directions: 1 = loading in axial compression leading to the blue point, whereby the deviatoric strain tensor and its rate have the same direction as illustrated in Fig. 2c; 2 = loading reversal from axial compression to axial extension or unloading leading to stress and strain reversal and to the red point, the deviatoric strain tensor

and its rate have opposite directions as illustrated in Fig. 2c; 3 = continued loading in axial extension leading to the green square. Eventhough the stress state of the green square coincides with the one of the blue point, the deviatoric strain tensor of the green square and its rate have certainly the same direction but nonetheless opposite to the ones of the blue point. For all states the deviatoric stress direction shows in the same direction but the stress increment direction is unknown. Thus, for the generalization of the *dilatancy* to multiaxial space, neither the stress tensor nor its unknown increment can be used. However, given the definition in **strain space** through Eq. 12, the most natural is to use the direction of the deviatoric strain rate, which is also in accordance with the observations presented in Fig. 2 and with the experimental behavior of sand reported for example in [5,10,21]. Thus, we propose a generalization of d considering the direction of the **strain rate** through its Lode angle $\theta_{\dot{\varepsilon}} = \theta_{\dot{\varepsilon}^*}$ (note that for the Lode angle calculation only the deviatoric component of the tensor is needed):

$$d = \frac{6 \sin \psi}{3 - \sin \psi \cos(3\theta_{\dot{\varepsilon}})} \tag{15}$$

and thus the stress ratio at the phase transformation line η_{PTL} which we will denote in general with M_d reads:

$$\eta_{PTL} = \frac{6 \sin \varphi_{PTL}}{3 - \sin \varphi_{PTL} \cos(3\theta_{\dot{\varepsilon}})} \overset{!}{=} M_d. \tag{16}$$

Note that Eq. 16 establishes the interrelation between the strain space and the stress space for the *dilatancy*. The phase transformation angle of friction φ_{PTL} will be discussed and defined in the next Section.

Furthermore, Pradhan et al. [5,10,21] studied the relationship between the dilatancy d and the stress ratio η of sand subjected to cyclic loading, whereby they postulate a unique relationship between the stress ratio and the *dilatancy* irrespective of void ratio and pressure level. During for example undrained cyclic loading the void ratio remains the same but the mean pressure changes resulting in a change of the critical void ratio. Hence, after a certain reduction of p the soil state is dense $e < e_c$ and when the stress state goes towards the phase transformation state $\eta \overset{!}{=} \eta_{PTL} = q_{PTL}/p_{PTL}$ both the mean stress and the deviatoric stress increase reaching a peak value. At the reversal point the stress path goes towards lower p and q viz. lower η with the greatest contractancy. Consequently, the *dilatancy* relation $d - \eta$ of each cycle may be alike in shape, but not the same because until $e > e_c$ $d \leq 0$ holds and when $e < e_c$ $d \overset{\geq}{\leq} 0$ holds depending on η. Yet, neither Pradhan et al. [5,10,21] nor the relations 7–9 consider the void ratio dependence of the *dilatancy*.

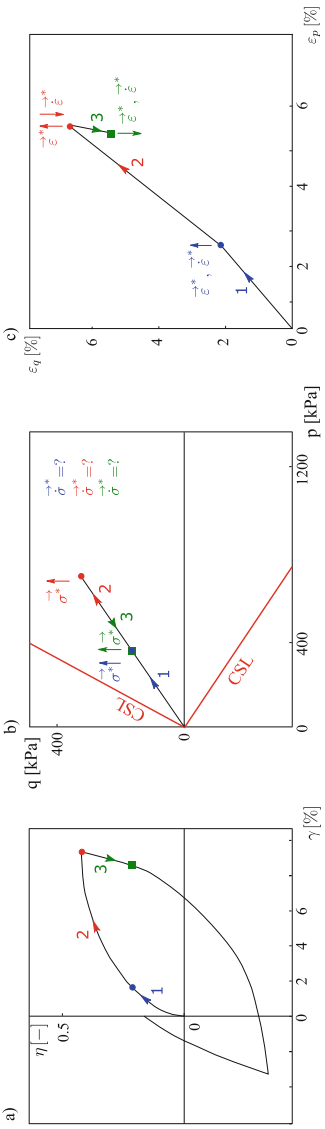

Fig. 2. Example of two different stress states (but three strain states) with different loading and straining directions: 1 = loading in compression, the deviatoric strain tensor and its rate have the same direction; 2 = loading in axial extension or unloading leading to stress and strain reversal, the deviatoric strain tensor and its rate have opposite directions; 3 = loading in extension leading to the green square. Eventhough the stress state of the green square coincides with the one of the blue point, the deviatoric strain tensor of the green square and its rate have certainly the same direction but nonetheless opposite to the one of the blue point. For all states the deviatoric stress direction shows in the same direction but the stress increment direction is unknown. (a) $\eta - \gamma$ space, (b) effective stress in $p - q$ plane, (c) $\varepsilon_p - \varepsilon_q$ space.

3 Overview of Expressions Describing the State-Dependent *Dilatancy* of Cohesionless Soils

Except of the state dependence, the *dilatancy* has to fulfill certain requirements arising from experimental evidence. On one side, at the phase transformation line (PTL) i.e. at $\eta = M_d$ the dilatancy vanishes $d(\eta = M_d) = 0$ [22]. On the other side, the critical state represents an ultimate state of failure at which $\eta = M$ and $e = const.$ thus no volumetric strain occurs. The constant volumetric strain $dv_d = 0$ implies $d(\eta = M, e = e_c) = 0$ at the critical state. A unique relationship between d and η would render $M = M_d$, which can represent an exceptional case for a certain value of e_0. However, in general laboratory data show that dense sand dilates $M_d < M$ and loose sand contracts $M_d > M$.

In the following we will review two approaches for the constitutive description of the state-dependent *dilatancy* of cohesionless soils.

3.1 State-Dependent *Dilatancy* for Monotonic Loading Described by Li and Dafalias [6]

In order to account for the density dependence of the *Dilatancy* for sands, Li and Dafalias [6] proposed a state-dependent expression for d:

$$d = \frac{d_0}{M} \left(M \exp(m\psi) - \eta \right), \quad \psi = e - e_c(p'). \tag{17}$$

The fulfillment of the critical state requirements for $e = e_c \Rightarrow \psi = 0$ and $\eta = M$ is evident. The second requirement $d(\eta = M_d) = 0$ implies a void ratio dependence of the phase transformation stress ratio $M_d = M \exp(m\psi)$.

The relationship proposed in Eq. 17 is illustrated in Fig. 3, whereby blue dots represent the experimental results of Pradhan et al. [5]. It is obvious that the relation given in Eq. 17 (orange lines in Fig. 3) is not in accordance with experimental evidence for axial extension. These disadvantages of Eq. 17 resulted in the introduction of the so-called fabric-dilatancy internal tensor-valued variable $\mathbf{z}$ by Dafalias and Manzari [23].

3.2 State-Dependent *Dilatancy* Described by Grandas and Triantafyllidis [24]

The dilatancy relation derived in Eq. 4 is void ratio independent and from Fig. 3 (purple lines) it can be observed that the Taylor's rule neither captures the strong contractancy upon reversals. To describe a state-dependent *Dilatancy* Grandas and Triantafyllidis [24] proposed a modification of the term describing the critical state $\tan \varphi_c$ analogous to the idea proposed by [6]. For this purpose the tangens of the critical state angle of friction is replaced by $\tan \varphi_{PTL} = \tan \varphi_c / f_e$, whereby f_e is a scalar function of void ratio and mean pressure. Some requirements has to be imposed on the formulation of the void ratio function f_e:

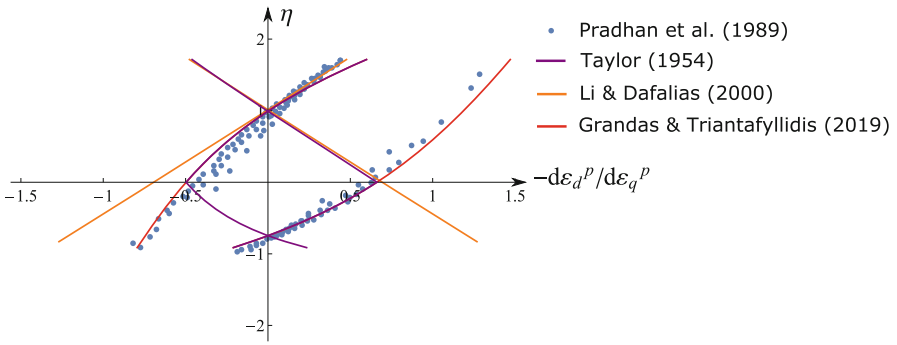

Fig. 3. Experimental results of constant pressure triaxial tests of Pradhan et al. [5] compared with the *dilatancy* relations proposed by Li and Dafalias [6] and Grandas and Triantafyllidis [24].

- if the mobilized state of the material is at failure i.e. the critical state is reached then $\varphi_m = \varphi_c$ and the dilatancy vanishes viz. $\psi = 0$. Thus, the void ratio function should render $f_e = 1$.
- when subjected to shearing, dense sand dilates which renders $M_d < M$. Hence, $\tan\varphi_{PTL} < \tan\varphi_c$ resulting in $f_e > 1$.
- loose sand upon shearing contracts and the phase transformation line lies then above the critical state line $M_d > M$ and may not be reached under monotonic loading. Thus, $\tan\varphi_{PTL} > \tan\varphi_c$ results in $f_e < 1$.

Equation 4 now reads:

$$\tan\psi = \tan\varphi_m - \tan\varphi_c / f_e. \tag{18}$$

Experiments evidence the maximum contractancy upon reversals of the strain path, see Fig. 3 and the reflections made in Sect. 2. This effect can be described by extending the dilatancy rule from Eq. 18 to account for the direction of shearing. A thermodynamically conform extension is proposed through the relation:

$$\tan\psi = \overrightarrow{\boldsymbol{\sigma}}^*{:}\,\overrightarrow{\dot{\boldsymbol{\varepsilon}}}^* \tan\varphi_m - \tan\varphi_c / f_e. \tag{19}$$

This relation is depicted in Fig. 3 with red lines and shows a perfect agreement with the experimental data of Pradhan et al. [5]. Thus, the *dilatancy* expressed by d or ψ is not only a function of stress as in Cam Clay theory $d = f(\boldsymbol{\sigma}, C)$ or from stress and void ratio as assumed by Li and Dafalias [6] $d = f(\boldsymbol{\sigma}, e, C)$, but also a function of the direction of shearing $\psi = f(\boldsymbol{\sigma}, e, \overrightarrow{\dot{\boldsymbol{\varepsilon}}}^*, C)$. Intrinsic material parameters denoted with C are of course included.

4 Experimental Findings Regarding the *Dilatancy* of Cohesive Soils

It is tentatively assumed that the *dilatancy* of fine-grained soils is only dependent on the stress ratio and on the intrinsic material parameters [25–29]. Yet,

experimental evidence gained for example in [9] shows that with increasing OCR resulting in a lower void ratio e_0 prior to the undrained monotonic shearing, the material response is rendered more dilative and an increase of the undrained shear strength is evidenced. For normalconsolidated samples the PTL may not be reached during shearing $M_d \geq M$ rendering the material response contractant. However, the PTL is observed to lie below the CSL for overconsolidated samples $M_d < M$. Similar dependencies of the *dilatancy* on the overconsolidation ratio can be concluded from the experiments presented in [12,30–40]. Nevertheless, the *dilatancy* effects and their dependence on the overconsolidation ratio, which is not trivial, was mostly ignored in the constitutive modeling of soft soils.

4.1 Basic Postulates

In order to proceed with some findings the therms normalconsolidated, lightly overconsolidated and heavily overconsolidated need to be defined. Consider isotropic states ($q = 0$) and isotropic loading directions ($\dot{q} = 0$) then the state of the material is defined by a combination of the void ratio e and the mean pressure p, whereby the normal consolidated state (OCR = 1) is given by the maximum void ratio e_i, see also Fig. 4:

$$e_i = e_{i0} - \lambda \ln(p/p_{ref}). \tag{20}$$

The slope of the normal consolidated line (NCL) in e vs. p diagram is determined through the compression index λ and its position is defined through the material constant e_{i0} specified at a reference mean pressure p_{ref}. Equation 20 can be solved for the void ratio equivalent normalconsolidated pressure imposing the condition $e = e_i$. Then, the relation proposed by Hvorslev [41] is obtained:

$$p_{ei} = \exp\left(\frac{e_{i0} - e}{\lambda}\right). \tag{21}$$

p_{ei} can be termed also as preconsolidation pressure (similarly to p_c in Cam Clay) and the formulation of its evolution rate is straightforward:

$$\dot{p}_{ei} = -\frac{\dot{e}}{\lambda} \exp\left(\frac{e_{i0} - e}{\lambda}\right) \tag{22}$$

Similarly to the NCL, the critical void ratio line in e vs. p diagram can be defined through:

$$e_c = e_{c0} - \lambda \ln(p/p_{ref,c}). \tag{23}$$

In analogy to sands and gravels, which are defined as loose or dense depending on the position of the state with respect to the critical void ratio line, also clays can be defined as lightly overconsolidated or heavily oversoncolidated. The analogy between the behaviour of grained and fine-grained soils has been depicted also in the pioneer work of Atkinson [42], but has been almost ignored in subsequent research. We define a material state lying between the NCL (OCR = 1)

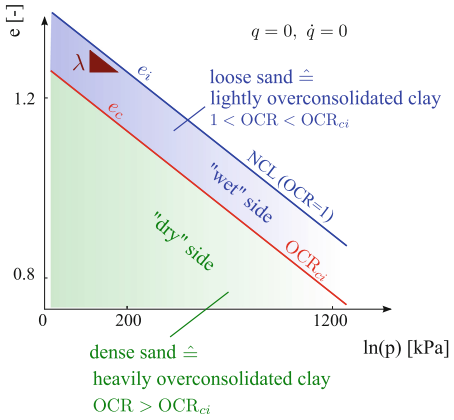

Fig. 4. State of soils for isotropic initial $q_0 = 0$ and isotropic loading conditions $\dot{q} = 0$.

and the critical void ratio line (OCR = $OCR_{ci} > 1$) (blue area in Fig. 4) as lightly overconsolidated ($1 < OCR < OCR_{ci}$), similar to the definitions in [42]. The subscript *ci* stays for the *c*ritical *i*sotropic line. The necessity for this definition will be clear after the generalization to three dimensional states in the next pages. However, the aforementioned states of soils are likely to be called on the "wet" side of the critical, not to be mixed up with the saturation of the soil. The soil is either saturated or dry and "wet" means that the void ratio e or the water content w at a mean pressure p is higher than the critical one e_c or more wet than the critical one w_c, respectively. For a heavily overconsolidated clay $OCR > OCR_{ci}$ (green area in Fig. 4) the void ratio is lower than the critical one. Therefore, the soil is termed on the "dry" side i.e. drier than at the critical line. These classifications correspond to the analogous characterisations of loose and dense sands. Note that only isotropic states $q = 0$ and isotropic loading directions $\dot{q} = 0$ are discussed above and illustrated in Fig. 4.

Now let us consider general stress states with $q \neq 0$. Then the soil is at its critical state when both the critical state line (CSL) $\eta = q_c/p_c \overset{!}{=} M$ and the critical void ratio line $e \overset{!}{=} e_c$ are reached. Eventhough the definition of the CS is "ordinary", the classification lightly or heavily overconsolidated is not straightforward. We first consider the state A in Fig. 5a on top, which is normalconsolidated. The most natural is to think that point A which is in e vs. p space uniquely defined, possesses infinite projections on the p vs. q plane along the line $p_A = const.$ Three marking states along this line are illustrated in Fig. 5a at the bottom: A1 at $q = 0$, A2 at $q < q_c$ and A3 at the critical state $q = q_c$. Each of these states are normalconsolidated if they are passed in the numbered order A1−A2−A3. In order to ensure uniqueness for general states we introduce the widely used concept of the loading surface. The (pre)loading surface represents a constant void ratio $e = const.$ and constant overconsolidation ratio surface which intersects the p-axis at $p = p_{ei}$ if OCR = 1. The critical state line and the loading

surface intersect each other at $p = p_{ei}/\mathrm{OCR}_{ci}$ and $q = \eta_c p$. Consequently, the points A1, A2 and A3 correspond to three different loading surfaces intersecting the p-axis at different mean preassures $p_{ei,A1} = p_A < p_{ei,A2} < p_{ei,A3}$. Figure 5(a and b) shows exemplary the loading surface for A1, which expands for the loading sequence A1–A2–A3 keeping the same shape. If they were projections of point A then $p_{ei,A1} = p_A = p_{ei,A2} = p_{ei,A3}$ would hold, which obviosly is in contradiction with the loading surface theory. Therefore, the projection of the NCL defined in $e - p$ space can be only realised for $q = 0$, hence in the isotropic axis of $p - q$ diagram and then A = A1 is uniquely defined in both spaces. If the initial state of the material corresponds to A2 and the sample is subjected to deviatoric unloading until the isotropic axis is reached, then the final state of the material is overconsolidated eventhough the void ratio and the mean stress remain unchanged $p_{ei,A2} > p_{ei,A1} = p_A$.

Secondly we will analyze states lying at the critical void ratio line denoted with point B in e vs. p diagram (Fig. 5a on top) having the same void ratio as A but lower mean pressure. Once more, one may think that infinite projections of B are possible in the $p - q$ space. In Fig. 5a on bottom, exemplary three of these projections are illustrated. Along the same lines of thoughts as for the NCL, also the critical void ratio line is to be projected at the isotropic axis. Thus, the unique projection of B corresponds to B1 ($q = 0$) and is equivalent to the states which separate the "wet" side from the "dry" side corresponding to a critical overconsolidation ratio OCR_{ci} (the subindex **ci** = **c**ritical **i**sotropic) in Fig. 4. For this purpose, we propose to define the critical void ratio as a shift by the OCR_{ci} of the maximum void ratio:

$$e_c = e_{i0} - \lambda \ln(\mathrm{OCR}_{ci}) - \lambda \ln(p/p_{ref}). \tag{24}$$

Thus, the loading surface can be constructed by knowing the current stress and void ratio of the material, current OCR and OCR_{ci} solely. The state B2 lies between $q = 0$ and $q = q_c$ and at a loading surface, which intersects the p-axis at $p^+_{ei,B2} > p^+_{ei,B1}$. Thus, B2 is characterised with a lower $\mathrm{OCR}_{B2} < \mathrm{OCR}_{B1} = \mathrm{OCR}_{ci}$ as on the "wet" side of the critical state. Point B3 lies at the critical state in the void ratio - pressure diagramm as well as in the effective stress plane. Because the critical state represents the "constant" state of the material and is independent of the initial state then it defines also a normalconsolidated state $\mathrm{OCR}_c = 1$. Considering these observations the isotropic critical overconsolidation ratio OCR_{ci} can be calibrated through an undrained shearing test of a normalconsolidated sample following the path A1–B3 $\Rightarrow \mathrm{OCR}_{ci} = p_{A1}/p_{B3}$. Note, that it is mandatory for the state B3 to fulfill both critical state requirements $e = e_c$ and $\eta = \eta_c$. Thus, in order to reach the critical state strains greater than 10% are needed, in some soils even greater than 50% [42].

Finally, we will consider the state C lying at the "dry" side of the critical void ratio line in Fig. 5(a). Its projection C1 on the $p - q$ plane, Fig. 5a is straightforward and corresponds to $\mathrm{OCR}_{C1} > \mathrm{OCR}_{ci}$ characterizing a heavily overconsolidated soft soil. For a state C2 ($q \neq 0$) lying inside the loading surface

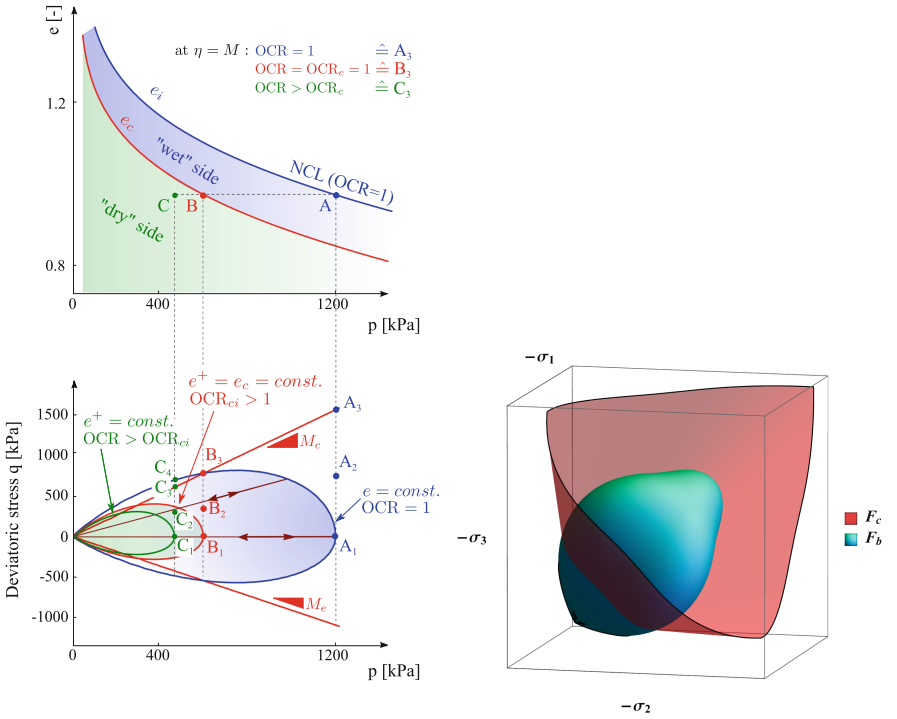

(a) State of soils for general initial and loading conditions $\dot{q} \neq 0$.

(b) Critical state surface F_c and bounding surface F_b in the principal stress space.

Fig. 5. Interrelation between the stress space and the void ratio space.

of B1 the overconsolidation ratio is less than at C1 but greater than the isotropic critical oversondolidation ratio $\mathrm{OCR}_{C1} > \mathrm{OCR}_{C2} > \mathrm{OCR}_{ci}$. Similarly, a state C3 lying outside the isotropic critical loading surface possesses $\mathrm{OCR}_{C3} < \mathrm{OCR}_{ci}$ characterizing a lightly overconsolidated soft soil. Eventhough C3 lies at the CSL $\eta = \eta_c$ the critical state is not reached as $e \neq e_c$. At long last, the state C4 lies at the initial or preloading surface reaching a peak stress q_p and $\mathrm{OCR}_{C4} = 1$. Thus state C, depending on the deviatoric stress q, can be characterized as all of them: heavily overconsolidated at C1 $p = 0$ and at C2 $0 < q < q(\mathrm{OCR} = \mathrm{OCR}_{ci})$, lightly overconsolidated at C3 $q(\mathrm{OCR} = \mathrm{OCR}_{ci}) < q < q(\mathrm{OCR} = 1)$ and normalconsolidated at C4 $q = q(\mathrm{OCR} = 1) = q_p$. Thus, for isotropic states Fig. 4 or Fig. 5a (e vs. p relationship) is sufficient in order to determine whether the soil is normal-, lightly- or highly consolidated. At anisotropic states, both the e vs. p relation and its generalization in $p - q$ space is necessary.

A lightly overconsolidated clay when subjected to shearing is expected to contract. We suggest that there is an overconsolidation ratio OCR_{ci} at which the soft soil behaviour changes from contractant $\mathrm{OCR} < \mathrm{OCR}_{ci}$ to dilatant (the material can both contract and dilate depending on η) $\mathrm{OCR} > \mathrm{OCR}_{ci}$ with the

PTL lying below the CSL, as will be shown through experiments in the next Sects. 4.2 and 4.3.

4.2 Triaxial Tests Under Monotonic Loading

In the last decades, many stress-*dilatancy* relations for sand have been proposed. An example therefore presents Fig. 3. For these studies, mostly constant pressure triaxial tests have been used, because then the volumetric change viz. the volumetric strain rate $\dot{\varepsilon}_v$[2] corresponds to the plastic one $\dot{\varepsilon}_v^p$. However, drained tests for clays are highly time-consuming and therefore very rare to find. For this reason, in this work we used undrained triaxial tests (monotonic and cyclic) of Kaolin Clay [14]. For the evaluation of its *dilatancy* behaviour some assumptions and relations need to be established.

In general, the volumetric strain rate consists of a *dilatancy* component $\dot{\varepsilon}_v^d$ and of an another component denoted with $\dot{\varepsilon}_v^c$:

$$\dot{\varepsilon}_v = \dot{\varepsilon}_v^c + \dot{\varepsilon}_v^d \tag{25}$$

$\dot{\varepsilon}_v^d$ is totally plastic and is induced by a plastic shear strain rate $\dot{\varepsilon}_q^p$, whereas $\dot{\varepsilon}_v^c$ contains both elastic and plastic components induced by the change in the effective mean stress p. Thus, the volumetric strain during tests with $p = const.$ is equally to the *dilatant* one:

$$\dot{\varepsilon}_v = \dot{\varepsilon}_v^p = \dot{\varepsilon}_v^d, \quad \text{for } p = const. \tag{26}$$

Similar relations are documented also by Shibata in [43]. Hence, a rearrangement of Eq. 6 is necessary for $p \neq const.$ The dilatancy is then defined as the relation between the dilatant volumetric strain increment (instead of total plastic one) and the plastic deviatoric strain increment:

$$d = -d\varepsilon_v^d / |d\varepsilon_q^p|. \tag{27}$$

Assuming that clays possess a unique normal consolidation line (NCL), then reloading occurs at nearly the same line (with (strain)hystheretical behaviour at the reverse direction) as the foregoing unloading did, see Fig. 6(a) and (b). For undrained conditions the total volumetric change vanishes $d\varepsilon_v = 0$ and hence the *dilatant* strain increment results from the prevention of the volumetric change and can be termed also prevented *dilatancy*. If the loading was not undrained, then the volumetric change would follow the unloading or unloading-reloading line for $\mathrm{OCR} \leq \mathrm{OCR}_{ci}$ or $\mathrm{OCR} > \mathrm{OCR}_{ci}$, respectively (marked with dark-green dottet line in Fig. 6(b)). On the other side, Fig. 6(c) and (d) show that sands do not behave the same way. Its compaction during for example isotropic unloading as presented in Fig. 6(c) leads to a new normal consolidation line lying below the first one (marked with dark-green dottet line in Fig. 6(d). Thus, the volumetric change upon subsequent undrained shearing goes along with the slope λ in the

[2] Note the equality $\dot{\square} = d\square/dt$.

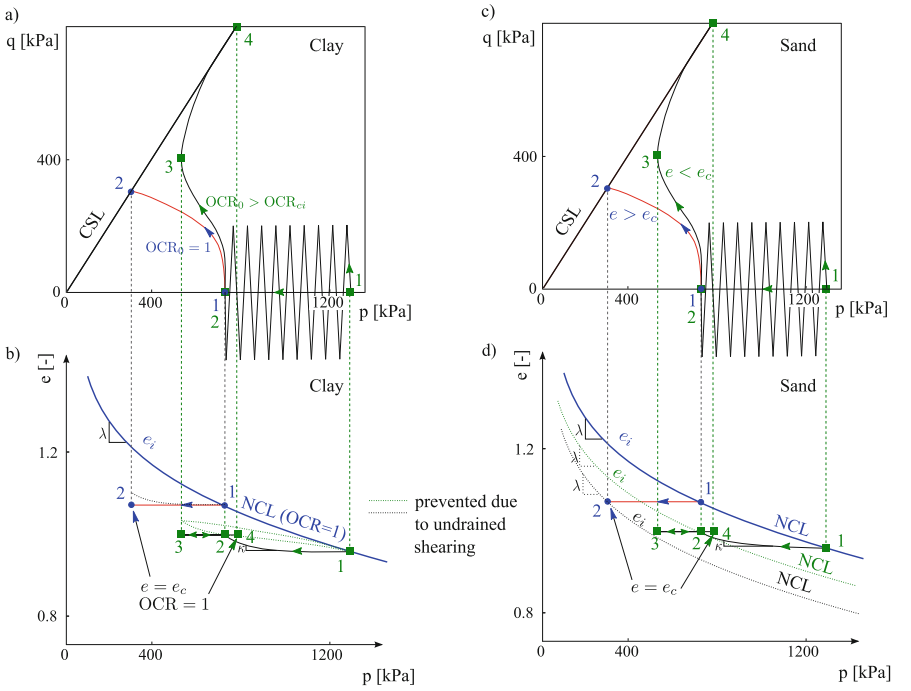

Fig. 6. Illustrative examples of isochoric shearing of a normalconsolidated ($\mathrm{OCR}_0 = 1$) and highly overconsolidated ($\mathrm{OCR}_0 > \mathrm{OCR}_{ci}$) clay sample (left) compared to a loose ($e_0 > e_{c0}$) and dense ($e_0 < e_{c0}$) sand sample (right). The overconsolidated clay sample or the dense sand sample are obtained by drained isotropic unloading until either $\mathrm{OCR}_0 > \mathrm{OCR}_{ci}$ or e_{c0}, in order to satisfy the requirement $e < e_{c0}$, are reached. In a) it is shown that when subjected to undrained shearing the normalconsolidated sample (blue point 1) is expected to contract (reaching blue point 2 at CSL) and a highly overconsolidated sample (dark-green square 2) to dilate after an initial contraction (reaching dark-green square 4 at CSL). These effects result due to the prevented *dilatancy* viz. if drained shearing occured then the unloading in the $e - \ln p$ space in (b) would follow the line with the slope κ. Therefore, also the dilatant behaviour starting from the dark-green square 3 in (a) and (b) would follow this line (marked with a dotted line in (b)) in the reverse direction rendering a totally elastic response at reloading until the NCL is reached. Thus for undrained shearing of clays holds: $\dot{\varepsilon}_v = \dot{\varepsilon}_c + \dot{\varepsilon}_d = \dot{\varepsilon}_{el} + \dot{\varepsilon}_d = 0 \Rightarrow \dot{\varepsilon}_d = -\dot{\varepsilon}_{el} = -\dfrac{\kappa \dot{p}}{p(1+e)}$. Sands however possess more than one NCL (depending on the initial void ratio e_0 and the loading history), hence after a compaction they always follow the line with the slope λ (new NCL) in the $e - \ln p$ space as demonstrated in (d) and thus $\dot{\varepsilon}_d \neq -\dot{\varepsilon}_{el}$ but $\dot{\varepsilon}_c = \dfrac{\lambda \dot{p}}{p(1+e)} = -\dot{\varepsilon}_d$.

$e - \ln p$ space consisting of a reversible part $d\varepsilon_v^{el}$ (belonging to the slope κ) and a plastic one $d\varepsilon_v^c + d\varepsilon_v^d$ (with the slope $\lambda - \kappa$). Following these realizations, for clays we suggest that the volumetric change due to the change in p is solely elastic $\dot{\varepsilon}_v^c = \dot{\varepsilon}_v^{el}$. Hence, the *dilatant* strain increment follows from:

$$d\varepsilon_v = d\varepsilon_v^{el} + d\varepsilon_v^p \quad \Rightarrow \quad d\varepsilon_v^d = d\varepsilon_v^p = -d\varepsilon_v^{el} \tag{28}$$

The elastic strain increment can be calculated from the constitutive equation:

$$\begin{bmatrix} dp^{el} \\ dq^{el} \end{bmatrix} = \begin{bmatrix} E_{pp} & E_{pq} \\ E_{qp} & E_{qq} \end{bmatrix} \begin{bmatrix} d\varepsilon_v^{el} \\ d\varepsilon_q^{el} \end{bmatrix} \tag{29}$$

$$\Rightarrow \begin{bmatrix} d\varepsilon_v^{el} \\ d\varepsilon_q^{el} \end{bmatrix} = \begin{bmatrix} C_{pp} & C_{pq} \\ C_{qp} & C_{qq} \end{bmatrix} \begin{bmatrix} dp^{el} \\ dq^{el} \end{bmatrix}. \tag{30}$$

Omitting the non-diagonal terms for an isotropic material and using the hypoelastic stiffness:

$$\mathsf{E}_{iso} = 3K \overrightarrow{\mathbf{1}}\overrightarrow{\mathbf{1}} + 2G\,\mathsf{I}^{dev} \tag{31}$$

one obtains:

$$d\varepsilon_v^{el} = dp/E_{pp} = \frac{2\lambda\kappa}{\lambda + \kappa}\frac{dp}{(1+e)p}. \tag{32}$$

Note that the void ratio during undrained shearing corresponds to the initial void ratio $e = e_0$.

For a transversal isotropic material the scaled hypoelastic stiffness can be used instead as proposed in [15]:

$$\mathsf{E}_{abcd} = \mathsf{Q}_{abij} : \mathsf{E}_{ijkl} : \mathsf{Q}_{klcd} \tag{33}$$

$$\mathsf{Q}_{abcd} = \mu_{ac}\mu_{bd} \tag{34}$$

$$\boldsymbol{\mu} = \sqrt{\alpha}\mathbf{1} + (1 - \sqrt{\alpha})\mathbf{m}_s \otimes \mathbf{m}_s, \tag{35}$$

with the vector along the sedimentation axis $\mathbf{m}_s$ and the material parameter α denoted as anisotropic coefficient [15]. For a vertical sedimentation axis viz. $\mathbf{m}_s = \{0, 0, 1\}$ corresponding to a vertically cutted Kaolin sample from [14] then the hypoelastic compliance from Eq. 30 in conjunction with the transversal isotropic hypoelastic stiffness given through Eqs. 33–35 reads:

$$C_{pp} = \frac{3K(\alpha-1)^2 + G(\alpha+2)^2}{27GK\alpha^2}$$

$$C_{pq} = \frac{(\alpha-1)(6\alpha K + 3K + 2G(\alpha+2))}{27\sqrt{2}GK\alpha^2}$$

$$C_{qp} = \frac{(\alpha-1)(6\alpha K + 3K + 2G(\alpha+2))}{27\sqrt{2}GK\alpha^2}$$

$$C_{qq} = \frac{4G(\alpha-1)^2 + 3K(2\alpha+1)^2}{54GK\alpha^2}$$

This set of equations present the basis for the evaluation of the experimental data published by Wichtmann and Triantafyllidis in [14]. Hereby we will discuss

both the evaluation procedure and the results of the monotonic tests on normal and overconsolidated samples OCR = {1, 2, 4, 8}. When trying to evaluate the data, the change of the mean pressure dp underlied a huge data scattet such that for example during some time points the same mean pressure was evaluated. This led to a vanishing *dilatancy* $d = 0$ for unrealistic stress ratios η and not even for a specific OCR_0 a unique relationship between $d - \eta$ could be established. For this reason, the development of the mean pressure was approximated through polynomial functions depending on the only equidistantly captured quantity i.e. the time t as follows:

$$p_{approx} = \sum_{i=0}^{n} a_i t^i, \quad \text{with} \quad 3 \leq n \leq 9. \tag{36}$$

The value of n was varied aiming the minimum residual of $(p_{approx} - p) \rightarrow 0.1$ kPa. The affinity of the curves represented another important criterium. For a transversal hypoelastic stiffness also the deviatoric stress q need to be approximated because its increment dq is used for the calculation of the irreversible components $d\varepsilon_v^d$ and $d\varepsilon_q^p$.

Finally, we will now discuss the results of the $d-\eta-\mathrm{OCR}_0$ relation. Figure 7a shows the relationship between the stress ratio and the dilatancy for different initial overconsolidation ratios OCR_0. It is evident that the normal consolidated sample $\mathrm{OCR}_0 = 1$ as well as the lightly overconsolidated sample $\mathrm{OCR}_0 = 2$ contracts $d < 0$ upon undrained compressive shearing $d\varepsilon_q > 0$, whereas the heavily overconsolidated samples with $\mathrm{OCR}_0 = 4$ and $\mathrm{OCR}_0 = 8$ dilate $d > 0$ for $d\varepsilon_q > 0$ after an initial contraction $d < 0$ for $d\varepsilon_q > 0$. The initial contraction decays with an increasing initial overconsolidation ratio. Hence the subsequent dilation increases and the phase transformation stress ratio $\eta = \eta_{PTL}$ at $d = 0$ is reduced. These observations form the basis for the classification of clays' *dilatancy* behaviour very similar to that of sands. The question arises which value can be assigned to OCR_{ci} (see Eq. 24) and whether it represents the same number for each clay. The Modified Cam Clay theory renders the value $\mathrm{OCR}_{ci} = \exp(1) = 2.71$ as a constant value. However, for the first we will let this value as a material parameter to be calibrated until we evaluate some cyclic undrained triaxial tests in the next Section.

Sands are classified as dense or loose in therms of their relative density value which would in this work coincide with the overconsolidation ratio for clays. The classification dependent on the void ratio itself is not the most appropriate for clays due to the experimental data scatter of the initial void ratio. On the other side, knowing the consolidation process and the preloading of the soil, the overconsolidation ratio can be determined by:

$$\mathrm{OCR} = \frac{p_{ei}}{p_{ei}^{+}} \tag{37}$$

with the Hvorslev stress p_{ei} defined in Eq. 21. To eleminate the data scatter of the initial void ratio one may use for $p_{ei} = \max(p)$ the maximum mean pressure the soil was subjected to. Here we of course assume that the loading history

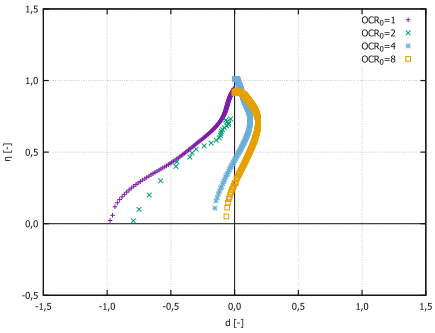

(a) Stress ratio η vs. dilatancy d relationship for different initial overconsolidation ratios OCR_0 evaluated from monotonic undrained triaxial tests performed on Kaolin. (Experiments borrowed from [14])

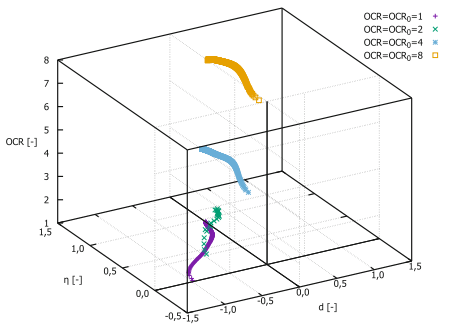

(b) $d-\eta-\mathrm{OCR}$ for the first approach $\mathrm{OCR} = \mathrm{OCR}_0 = const.$

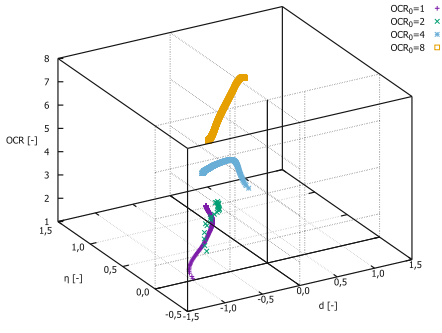

(c) $d-\eta-\mathrm{OCR}$ for the second approach $\mathrm{OCR} = p_e/p$.

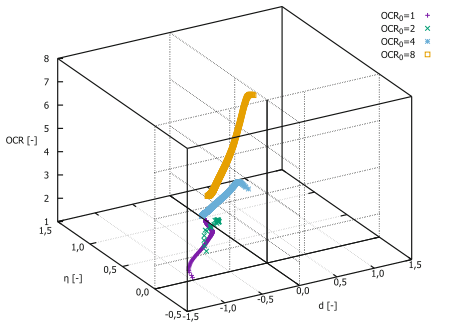

(d) $d-\eta-\mathrm{OCR}$ for the third approach $\mathrm{OCR} = p_e/p_{ei}^{+}$.

Fig. 7. Two- and three-dimensional relation between $d-\eta-\mathrm{OCR}$ evaluated from monotonic undrained triaxial tests performed on Kaolin. (Experiments borrowed from citewt17)

of the soil is known, which is mostly the case with reconstituted samples. Now three different approaches for the definition of the mean pressure corresponding to the actual void ratio of the soil p_{ei}^{+} are presented. Firstly, as a very simple but also a very rough approximation can serve $\mathrm{OCR} = \mathrm{OCR}_0$ thus $p_{ei}^{+} = p_{ei}$ and $\mathrm{OCR} = const.$ during the undrained shearing. The evaluated data corresponding to this (absurde) assumption is presented in Fig. 8a and b. Thus, the critical state $\mathrm{OCR} = 1$ and $\eta = \eta_c$ for initially overconsolidated samples $\mathrm{OCR}_0 \neq 1$ will never be reached in therms of OCR.

Secondly, as a more natural, appropriate and still simple but as will be explained not ideal approach one can approximate the mean pressure corresponding to the actual isotropic stress state ignoring the influence of the

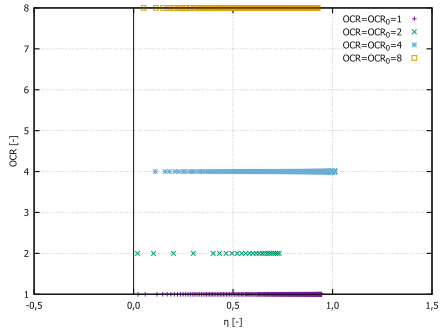

(a) OCR $-\eta$ space for the first approach OCR = $\mathrm{OCR}_0 = const.$

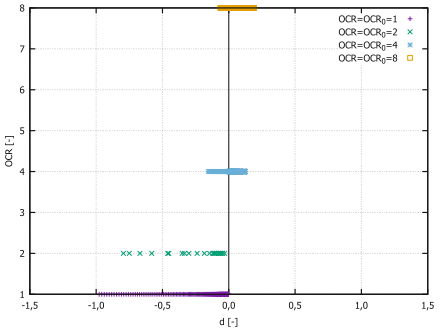

(b) OCR vs. d plane for the first approach OCR = $\mathrm{OCR}_0 = const.$

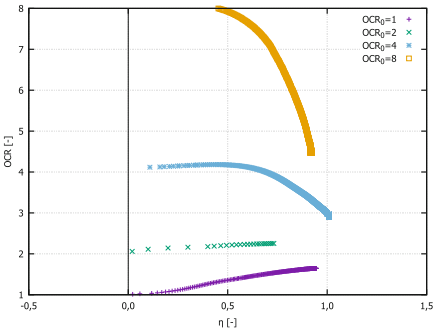

(c) OCR$-\eta$ space for the second approach OCR = p_e/p.

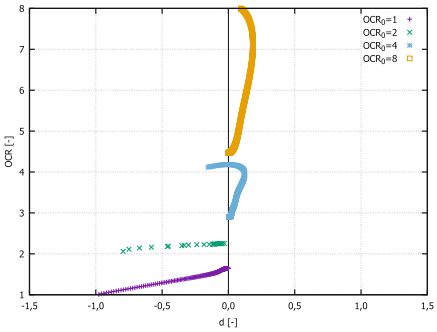

(d) OCR vs. d plane for the second approach OCR = p_e/p.

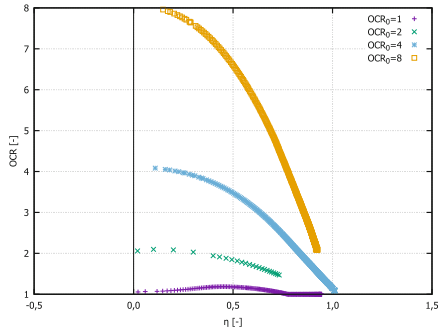

(e) OCR $-\eta$ space for the third approach OCR = p_e/p_{ei}^{+}.

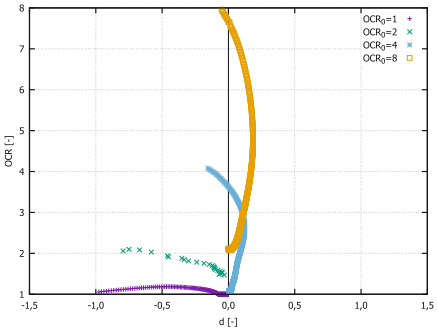

(f) OCR vs. d plane for the third approach OCR = p_e/p_{ei}^{+}.

Fig. 8. OCR$-\eta$ and OCR$-d$ relationships evaluated from monotonic undrained triaxial tests performed on Kaolin with different OCR definitions. (Experiments borrowed from [14])

deviatoric stress viz. $p_{ei}^{+} = p$. Figure 8c and d present the results for this approach in $\mathrm{OCR} = p_e/p$ vs. η space and in $\mathrm{OCR} - d$ plane, respectively. An increase of OCR for the normalconsolidated sample can be observed during the shearing. If the postulate that normalconsolidated samples contract when subjected to undrained shearing holds, then with this approach the critical state line implying $\mathrm{OCR} = 1$ and $\eta = \eta_c$ will never be reached for initially normalconsolidated samples. More controversial is the fact that an initially normal consolidated sample becomes overconsolidated during undrained shearing. As one might expect, the initially overconsolidated samples are not able to reach the CSL for this evaluating approach neither. One may build a conceptual case when $\mathrm{OCR} = 1$ can be reached then the dilation must be so large that the mean pressure reachs its initial value $p \geq p_0$. To the authors knowledge this behaviour is not supported by any experimental evidence.

Finally, we suggest for the definition of p_{ei}^{+} the same relation we already proposed in [15,44]:

$$p_{ei}^{+} = \exp\left(\frac{e_{i0} - e^{+}}{\lambda}\right) \tag{38}$$

Therefore the loading surface relation from [15,44] is solved for the void ratio e^{+} corresponding to the actual stress state:

$$e^{+} = A^{1/n_f}\, e_i, \quad A = 1 - \left(\frac{|\eta|}{M f_{b0}}\right) \tag{39}$$

$$n_f = \frac{\ln(f_{b0}^2 - 1)/f_{b0}^2}{\ln(e_c/e_i)} \tag{40}$$

with the bounding surface material parameter f_{b0}. This formulation of the bounding surface and of OCR is also used for the explanations presented in Fig. 5b. The dilatancy relationships for Kaolin are once more for this approach illustrated in Fig. 8e and f. Hereby the consistency with the critical state surface is evident, hence the critical state is reached when $\mathrm{OCR} = 1$ is obtained. Note, that this limit state is reached only when $\eta = \eta_c$ (which arises also from the limit calculation $\lim_{\eta \to \eta_c} \mathrm{OCR} = 1$). Thus $\mathrm{OCR} = 1$ represents a sufficient condition for the CSL! Fig. 8e and f indicate that for the sample with $\mathrm{OCR}_0 = 8$ the critical state is not reached yet which is in accordance with the documentation in [14]. In [42] Atkinson explained: "The critical state will normally be reached after strains greater than 10%."... At this stage "the movements of grains are essentially turbulent, involving relative movements and rotations of both clay and sand grains. At larger displacements, however, the strains become localized into distinct zones of intense shearing and the shear stresses applied to the clay soil decrease." Thus, it is likely that for this sample the critical state was not reached, but a sort of "laminar flow" of flat clay grains which became parallely oriented to a very thin shearing zone occured. Furthermore, the limits of the application of continuum theory are reached in this case.

Figures 7b, c and d present the above discussed relations in the three-dimensional space $d - \eta - \mathrm{OCR}$. Once more it is evident that the third approach

presented in Fig. 7d renders both $d = 0$ and OCR $= 1$ at the critical state, following the first approach illustrated in Fig. 7b the CSL will never be reached and according to the second approach in Fig. 7c both the CSL is reached under controversial conditions and the development of OCR for example for initially normal consolidated samples is very unrealistic. Note that these observations along with Eqs. 37, 38, 38, 40 and $p_{ei} = p_0$ (for initially isotropically consolidated samples) represent a sufficient condition for the CSL, avoiding the experimental void ratio scatter. Thus, the OCR value calculated through Eq. 37 is a very good indicator whether the ultimate state is reached or not.

4.3 Triaxial Tests Under Cyclic Loading

A cyclic undrained triaxial test named C08 and presented in [14] is evaluated for the *dilatancy* relation in the following. With a constant rate of axial strain $\dot{\varepsilon}_1 = 0.12/\text{h}$ and a deviatoric amplitude of $q_{ampl} = 70$ kPa the sample could withstand nearly 7 cycles until the failure criterion of $|\varepsilon_1| = 10\%$ is reached. For purposes of the *dilatancy* evaluation, the cycles are separated according to the direction of the shear strain increment $\Delta\gamma$ (separation points correspond to the loading direction reversals) in 0.5 units beginning with 0.25. An essential point (for all time-depentent materials) is that the shearing velocity was held constant during the test to $||\Delta\gamma|| = 0.0113 = const.$ corresponding to $\Delta\gamma = 0.0113$ at loading in axial compression (the sample is axially compressed) and $\Delta\gamma = -0.0113$ at unloading in axial compression (the sample is axially extended).

Two different approaches are used for the calculation of elasticity. First the isotropic hypoelasticity as described in [20] is adopted. The compression index λ and the swelling index κ are calibrated to fit the oedometric tests: λ as the slope of the virgin compression line and κ the average slope of the unloading-reloading hystheresis. The initial void ratio in the evaluation was adjusted to account for the initial overconsolidation ratio $e_0 = e_{i0} - \lambda \ln(p_0 \cdot \text{OCR}_0)$. The authors of the experiments [14] reported normalconsolidated sample for C08, thus $\text{OCR}_0 = 1$. The maximum void ratio e_{i0} was calibrated at a reference pressure of $p_{ref} = 1$ kPa for the OCR $= 1$ isotache, as described in [15,20,45]. Secondly, the transverse isotropic hypoelasticity as introduced by the authors in [15,44] is utilized. Therefore, the calibration of the anisotropic coefficient α is required. A calibration scheme of α in conjunction with the Poisson ratio ν is also given in [15,44]. Table 1 lists the parameters' values used for the evaluation of the elasticity in C08.

Finally, Fig. 9 shows the resulting *dilatancy* relations. Note that throughout all these figures $d = -d\varepsilon_v^d / d\gamma^{tot}$ has been used in order to provide a more comparative study with the results of Pradhan et al. for sand [5]. To obtain the relation described in Eq. 6 a factor of 3/2 ($\varepsilon_q = 2/3\gamma$ for triaxial conditions) should be introduced which would solely elongate the *dilatancy* curves. In absence of $p' = const.$ tests with intermediate small loops of unloading and reloading, γ^{tot} presents a good approximation for γ^p. Further research in this point is required. The figures on the left side (Figs. 9a, c and e) accounted for

Table 1. Parameters used for the elasticity evaluation in C08

Elasticity approach	ν [−]	α [−]	λ [−]	κ [−]	e_{i0} [−]
Hypoelasticity	0.3	–	0.13	0.05	1.76
Transverse isotropic hypoelasticity	0.3	1.8	0.13	0.05	1.76

hypoelasticity, while the figures on the right side (Figs. 9b, d and f) for the transverse isotropic hypoelasticity. It is to be noted, that when the loading direction was reversed the different approaches did not yield the same behaviour. By comparing the Figs. 9a, b, c, d, e and f the following points may be noticed.

- Considering all cycles Figs. 9a and c (hypoelasticity used), b and d (transverse isotropic hypoelasticity used) the $d - \eta$ relation is different among different loading cycles, especially at loading reversals in axial extension. Differences between the elasticity approaches may be observed intensively comparing Figs. 9a or c with b or d, respectively. While using the hypoelasticity the points at loading reversals from axial compression to axial extension jump all to the dilatant area. Yet, Kaolin turned out to be transverse isotropic as showed in [15,20,44], thus the usage of transverse isotrope hypoelasticity would provide a more representative approach for Kaolin. Then, it can be observed that among some data scatter the loading reversals from axial compression to axial extension jump to the contractant area as observed also for sands. Note that no data points has been omitted during these evaluations.
- Figures 9e and f account only for regular cycles. The scattering in the relation is no longer present. As discussed also before it is now in fact more obvious that accounting for hypoelasticity the loading reversal $\Delta\gamma > 0 \rightarrow \Delta\gamma < 0$ renders dilatancy, whereas using transverse isotropic hypoelasticity it results in dilatancy, which is conform with the findings for sand in [5]. The shape of the curves is also different comparing both elasticity approaches. It may be concluded once more that the transverse isotropic hypoelasticity corresponds better to the behaviour of Kaolin.
- Pradhan et al. [5,10,21] claimed that using $d\gamma^p$ instead of $d\gamma^{tot}$ would reduce the scattering in the relations for sand. We however observe a scattering in the first (non regular cycles), see Figs. 9e and f. The scattering in the first and intermediate cycles can possibly be reduced by using $d\gamma^p$.
- The "elastic dilatancy" in reversals evident for example in Fig. 9c, which is eliminated using the transverse isotropic hypoelasticity, see for example Fig. 9d, provokes an increase of the effective mean stress resulting in a slope to the upper left of the effective stress path [14,15,44]. It is well known that clays possess a greater elastic locus compared to sands. If the elasticity was isotropic than the described $p - q$ path would be vertical with respect to $p-$axis. Thus, we can call the inherent anisotropy responsible for an even lower excessive pore water pressure after loading reversal. Sands in contrast react with the "highest" contraction after loading reversal. Hence, the greater

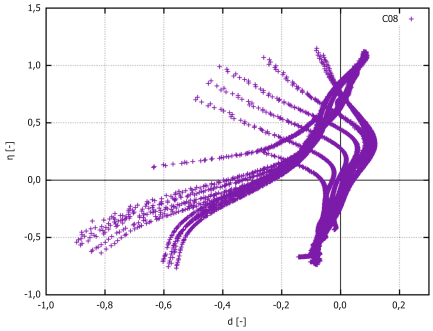

(a) All cycles. It was accounted for the isotropic hypoelasticity.

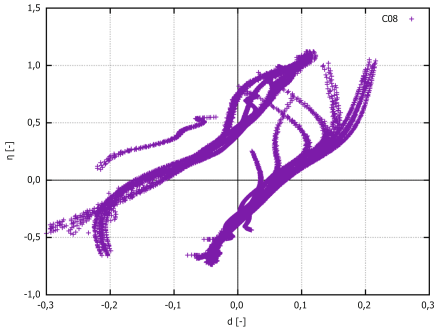

(b) All cycles. It was accounted for the transverse hypoelasticity.

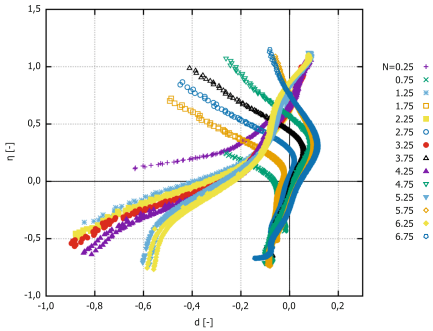

(c) Cycles separated in 0.5 cycles. It was accounted for the isotropic hypoelasticity.

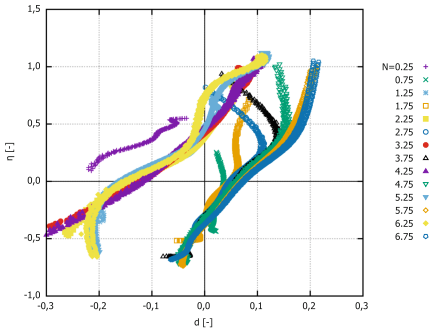

(d) Cycles separated in 0.5 cycles. It was accounted for the transverse hypoelasticity.

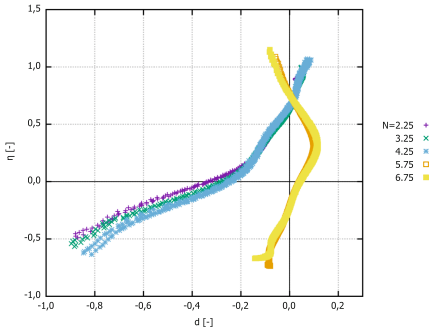

(e) Only regular cycles are plotted. It was accounted for the isotropic hypoelasticity.

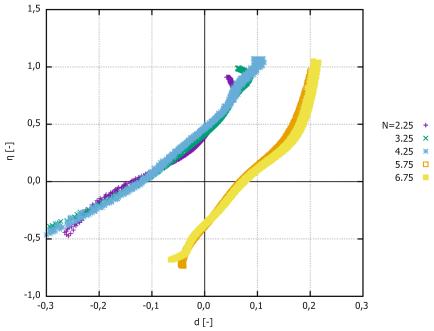

(f) Only regular cycles are plotted. It was accounted for the transverse hypoelasticity.

Fig. 9. d-η relationship evaluated for C08. (Experiment borrowed from [14])

elastic regime cannot be overcomed through the contractancy and thus results in a non vanishing mean pressure at cyclic mobility $p' \neq 0$. This effect can be implified with the inherent anisotropy according to the sedimentation axis. Thus, a cutting direction of the sample may be found at which the soft soil would also liquify (weak axis). The last assumption requires further research. Some authors explain the non-liquefaction behaviour of clays with the viscosity and its cohesive effect. If this was supposed to be truth, than the intensity of creep would not vanish with higher over consolidation ratio as has been experimentally documented in [28,46]. On the other side, it implies the existence of a special strain rate (loading velocity) with which the cyclic undrained shearing of a clay sample would result in liquefaction. Following our theory this would be the case for the greatest velocity $\dot{\varepsilon}_1 \rightarrow \infty$, hence the viscous effects wouldn't have time to develope. The experimentes presented in [14] and the discussions made in [44] give a hint to this phenomenon. However, further research work is required in order to bring more light and explain this phenomenon.

- With the undrained cyclic loading of normal consolidated samples the overconsolidation ratio increases and the stress ratios at the phase transformation line M_{dc} and M_{de} from Eq. 16 appears to be not affected as illustrated in Figs. 9e and f. Considering the non-regular cycles, Figs. 9a–d, η_{PTL} seems to increase with the number of cycles in axial extension. Such effects has not been reported in the literature, moreover the monotonic tests illustrated in Figs. 8 and 7 show opposite behaviour (but only for axial compression, no monotonic tests were available for axial extension). Further research works are required at this point.

In general, we can conclude that following the experimental evidence gained on Kaolin in [14] and evaluated in this work the *dilatancy* is a function of the stress ratio η and the void ratio e along with the intrinsic material parameters summarized under C, hence $d = f(\eta, e, C)$. Furthermore, we proposed an OCR-definition in Eq. 37, which includes the influence of both the stress ratio and void ratio such that $d = f(\text{OCR}, C)$.

If the assumption $d = f(\eta, C)$ would hold, the direction of plastic flow influencing the direction of the undrained stress path would be able to render dilatant direction only for $\eta = M \Rightarrow M_d = M$ independent of the overconsolidation ratio of the material. Thus, the same behaviour would be obtained for each OCR contradicting the findings gained in experiments and explained in this Section as illustrated in Figs. 7, 8 and 9.

5 Constitutive Description of the Dilatancy of Cohesive Soils

Perusal of actual research works regarding constitutive modeling of soft soils suggest that for clays a unique relation between the *dilatancy* d and the stress ratio η exist. This relation was used by the Cam Clay theory $d = M - \eta$ in [25]

or $d = (M^2 - \eta^2)/\eta$ [26] resulting in a dilative response only when the stress ratio reaches the critical state line thus $M_d = M$. Similarly, the hypoplastic model developed by Masin [27] is able to reproduce dilatant behaviour only for states lying above the critical state. The usage of a unique relation between d and η is reported as satisfactorily for cohesive soils by some authors [6,27]. This assumption may be consistent for normalconsolidated clays subjected to monotonic loading. However, we showed in Sects. 4.2 and 4.3 that the overcritical dilation is not sufficiently described for general initial states of cohesive soils and the less for cyclic loading.

5.1 Incorporation in a General Hypoplastic Model

We start with the *dilatancy* relation given in Eq. 6. Note the difference between this definition of d and the one determined by Pradhan et al. in [5,10] $d = -d\varepsilon_v^p/|d\gamma^p|$ with $d\gamma = 3/2 d\varepsilon_q$. For multiaxial generalization purposes we will however stick to our formulation, Eq. 6, which can be rearranged to:

$$d = -\frac{\mathrm{tr}(\dot{\boldsymbol{\varepsilon}}^p)}{\sqrt{2/3}\,||\dot{\boldsymbol{\varepsilon}}^{*p}||} \;\Rightarrow\; -\mathbf{1} : \dot{\boldsymbol{\varepsilon}}^p = d\sqrt{2/3}\,||\dot{\boldsymbol{\varepsilon}}^{*p}|| \tag{41}$$

with the deviator of the plastic strain rate $\dot{\boldsymbol{\varepsilon}}^{*p}$. The *dilatacy* evaluated on sands rendered a similar relationship when using $d\varepsilon_q$ instead of $d\varepsilon_q^p$. In particular, eventhough the scattering of the data is reduced when using $d\varepsilon_q^p$, it was very difficult to evaluate d after the loading reversal, because when both values $d\varepsilon_v^p$ and $d\varepsilon_q^p$ are very small $||\dot{\boldsymbol{\varepsilon}}|| < 10^{-5}$ it can be defined also as completely elastic regime [5]. Similar effects are shown in Sect. 4.3 for the behaviour of clays. Moreover, for the evaluations presented in Figs. 7, 8 and 9 we used the total deviatoric strain rate instead of the plastic one, thus in Eq. 41 we can substitute $||\dot{\boldsymbol{\varepsilon}}^{*p}|| \approx ||\dot{\boldsymbol{\varepsilon}}^{*}||$ to obtain:

$$-\mathbf{1} : \dot{\boldsymbol{\varepsilon}}^p = d\sqrt{2/3}\,||\dot{\boldsymbol{\varepsilon}}^{*}||. \tag{42}$$

From the point of view of a constitutive equation, the plastic strain rate has to be identified from Eq. 41. We start by expressing $\dot{\boldsymbol{\varepsilon}}^p$ by its isotropic and deviatoric components with unknown magnitudes a and b respectively:

$$\dot{\boldsymbol{\varepsilon}}^p = a\mathbf{1} + b\,\vec{\dot{\boldsymbol{\varepsilon}}}^{*p} \tag{43}$$

By multiplying both sides from left of Eq. 43 with 1 and inserting Eq. 42 we obtain for the isotropic magnitude a:

$$\mathbf{1} : \dot{\boldsymbol{\varepsilon}}^p = 3a \overset{42}{=} -d\sqrt{2/3}\,||\dot{\boldsymbol{\varepsilon}}^{*}|| \tag{44}$$

$$\Rightarrow a = -\frac{1}{3}\sqrt{\frac{2}{3}}\,d\,||\dot{\boldsymbol{\varepsilon}}^{*}||. \tag{45}$$

Inserting Eq. 45 and $b = ||\dot{\boldsymbol{\varepsilon}}^{*p}|| \approx ||\dot{\boldsymbol{\varepsilon}}^{*}||$ in Eq. 43 and dividing both sides of Eq. 43 with $||\dot{\boldsymbol{\varepsilon}}^{*}||$ renders the following relation for $\dot{\boldsymbol{\varepsilon}}^p$:

$$\frac{\dot{\boldsymbol{\varepsilon}}^p}{||\dot{\boldsymbol{\varepsilon}}^{*}||} = -\frac{1}{3}\sqrt{\frac{2}{3}}\,d\,\mathbf{1} + \vec{\dot{\boldsymbol{\varepsilon}}}^{*}\,. \tag{46}$$

For the derivation of Eq. 46 the assumption $\overrightarrow{\dot{\boldsymbol{\varepsilon}}^{*p}} \approx \overrightarrow{\dot{\boldsymbol{\varepsilon}}^{*}}$ was involved as well. Finally the well known hypoplastic constitutive equation:

$$\dot{\boldsymbol{\sigma}} = \mathsf{E} : \left(\dot{\boldsymbol{\varepsilon}} - \dot{\boldsymbol{\varepsilon}}^{hp} \right) = \mathsf{E} \left(\dot{\boldsymbol{\varepsilon}} - Y \mathbf{m} ||\dot{\boldsymbol{\varepsilon}}|| \right) \tag{47}$$

is considered. The viscous strain rate is without loss of generality disregarded in respect thereof. Drawing parallels between the plastic (Eq. 46) and the hypoplastic strain rate (Eq. 47) explicit relations for the flow rule and the degree of nonlinearity are obtained:

$$\mathbf{m} = \left(-\frac{1}{3}\sqrt{\frac{2}{3}}\, d\, \mathbf{1} + \overrightarrow{\dot{\boldsymbol{\varepsilon}}^{*}} \right)^{\rightarrow} \tag{48}$$

$$Y_D = \frac{||\dot{\boldsymbol{\varepsilon}}^{*}||}{||\dot{\boldsymbol{\varepsilon}}||} \left\| -\frac{1}{3}\sqrt{\frac{2}{3}}\, d\, \mathbf{1} + \overrightarrow{\dot{\boldsymbol{\varepsilon}}^{*}} \right\|. \tag{49}$$

The last relation defining Y can be simplified to read:

$$Y_D = \sqrt{1 - \frac{1}{3}\frac{\mathrm{I}_1^2(\dot{\boldsymbol{\varepsilon}})}{\mathrm{I}_1(\dot{\boldsymbol{\varepsilon}}^2)}} \left\| -\frac{1}{3}\sqrt{\frac{2}{3}}\, d\, \mathbf{1} + \overrightarrow{\dot{\boldsymbol{\varepsilon}}^{*}} \right\| \tag{50}$$

Note that the relation 50 serves only to define the degree of nonlinearity for shearing and should not be mixed up or used for the isotropic or radial compression. For radial compression Y_I the relations proposed in [15,20,44,47] or in [24] can be used for clays or sands, respectively. An interpolation function between Y_I for isotropic states and radial loading directions and Y_D for shearing is convenient.

A fundamental drawback of the flow rule presented in Eq. 48 is the deviatoric direction. For hypoplastic models a deviatoric direction of the flow rule equally to the deviatoric direction of the strain rate would mean that at loading reversals from stress states lying at the critical state the flow rule would try to get the stress state outside the critical state (or the bounding surface if introduced). The FE-simulation would loose the controllability and abort the calculation. Moreover, experimental observations show indeed deviatoric flow direction at the critical state but corresponding to the direction of the deviatoric stress. For this purpose a modified flow rule for hypoplastic models will be used:

$$\mathbf{m} = \left(-\frac{1}{3}\sqrt{\frac{2}{3}}\, d\, \mathbf{1} + \left(\frac{\overrightarrow{\boldsymbol{\sigma}^{*}}}{p} \right) \right)^{\rightarrow} \tag{51}$$

For the stiffness tensor E in Eq. 47 the hypoelastic stiffness from [15,44,47] is adopted. The equations of the reference model presented in [44] which are ommitted in this section are therefore summarized in the Appendix.

5.2 Simulations

Now the simulations compared with the experimental results (borrowed from [14]) which are reviewed, evaluated and discussed in Sects. 4.2 and 4.3 are shown. For the different tests the same set of material parameters, listed in Table 2, has been used.

Table 2. Material parameters

ν	α	λ	κ	e_{i0}	M_c	f_{b0}	n_{PTL}	n_{OCR}	χ	I_v
0.3	1.8	0.13	0.05	1.76	1.0	1.5	3	2	20	0.025

Figure 10 presents the simulations of the monotonic undrained triaxial tests with different initial overconsolidation ratios $\mathrm{OCR}_0 = \{1, 2, 4, 8\}$, whereby the dilatant behaviour is evident for higher $\mathrm{OCR}_0 > 2$. These tests are also used for the evaluations in Sect. 4.2. The simulations show very good agreement with the experimental results in both effective stress paths (right figure) and deviatoric stress vs. axial strain space (left figure). The shearing at strains greater than approximately 12% can provoke inhomogenity of the sample and localization of shear strains, thus it was not considered by the model. In the $q - \varepsilon_1$ space it corresponds to the softening of the deviatoric stress evident in the experimental curves. Furthermore, the inherent anisotropy of Kaolin is captured well by the model as can be seen from the simulation for $\mathrm{OCR}_0 = 1$.

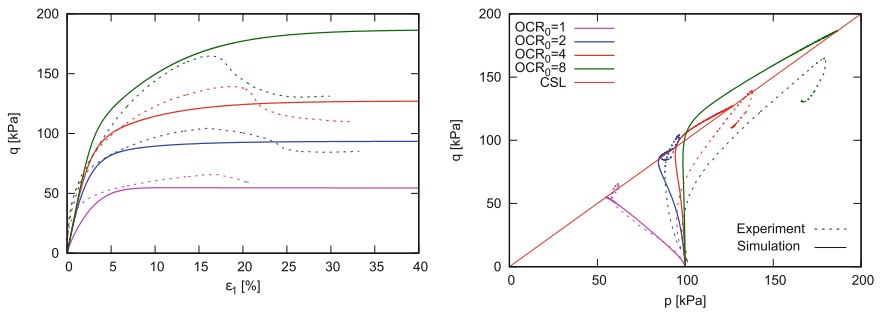

Fig. 10. Experimental results from [14] and simulations with the proposed model of undrained triaxial tests with variation of the initial overconsolidation ratio $\mathrm{OCR}_0 = \{1, 2, 4, 8\}$. The displacement rate was held constant in each test to $\dot{s} = 0.025$ mm/min. The laboratory tests are presented with dashed lines, whereas the simulations with solid lines.

Figure 11 presents an undrained triaxial cyclic test of a normalconsolidated sample $\mathrm{OCR}_0 = 1$ with deviatoric amplitude of $q_{ampl} = 70$ kPa. The failure criterion for the experiment was defined as an axial strain of 10%. The simulation

in $q-\varepsilon_1$ space is in good accordance with the experimental findings. Furthermore, the hysteresis when reaching the cyclic mobility is satisfactorily described. The same conclusions can be drawn for the effective stress path whereby 7 cycles has been surpassed. The 8-shaped cyclic mobility of the $p-q$ path is in good agreement with the experiment.

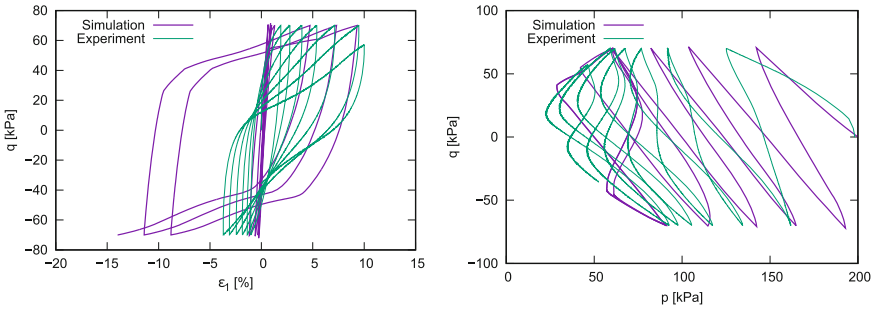

Fig. 11. Experimental result from [14] and simulation with the proposed model of a cyclic undrained triaxial test with constant displacement rate $\dot{s} = 0.1\,\mathrm{mm/min}$ and deviatoric amplitude of $q_{ampl} = 70\,\mathrm{kPa}$.

6 Concluding Remarks

This work provides a new evaluation method of the *dilatancy* from monotonic and cyclic undrained triaxial tests. Herein it has been realized for the experiments performed on Kaolin [14]. In general we can conclude that leastwise for this soft soil the *dilatancy* is a function of the stress ratio η and the void ratio e along with the intrinsic material parameters (as observed for sands). Furthermore, we proposed an OCR-definition, which includes the influence of both the stress ratio and void ratio such that $d = f(\mathrm{OCR}, C)$. We suggest that there is an overconsolidation ratio OCR_{ci} at which the soft soil behaviour changes from contractant $\mathrm{OCR} < \mathrm{OCR}_{ci}$ to dilatant (the material can both contract and dilate depending on η) $\mathrm{OCR} > \mathrm{OCR}_{ci}$ with the PTL lying below the CSL, as was also shown in the present study. We further proposed a constitutive relation describing the behaviour of soft soils including the *dilatancy* and viscosity. Some simulations of monotonic as well as cyclic tests are shown.

In order to verify these results for plastic clays, soft soils with higher plasticity should be evaluated in a subsequent work. In addition laboratory tests with constant mean pressure are required for the improvement of the *dilatancy* relation for cohesive soils.

Acknowledgements. The financial support from the German Research Community (DFG TR 218/27-1) is herewith gratefully acknowledged.

Appendix

Constitutive model

Constitutive equation:

$$\dot{\boldsymbol{\sigma}} = \mathsf{E} : \left(\dot{\boldsymbol{\varepsilon}} - \dot{\boldsymbol{\varepsilon}}^{hp} - \dot{\boldsymbol{\varepsilon}}^{vis}\right) \tag{52}$$

Elasticity:

$$\mathsf{E}^{iso} = 3K\ \vec{\mathbf{1}}\vec{\mathbf{1}} + 2G\,\mathsf{I}^{dev} \tag{53}$$

$$\mathsf{E}_{abcd} = \mathsf{Q}_{abij} : \mathsf{E}_{ijkl} : \mathsf{Q}_{klcd} \tag{54}$$

$$\text{with} \quad \mathsf{Q}_{abcd} = \mu_{ac}\mu_{bd} \quad \text{and} \quad \mu = \sqrt{\alpha}\mathbf{1} + (1-\sqrt{\alpha})\mathbf{m}_{\mathrm{s}} \otimes \mathbf{m}_{\mathrm{s}}. \tag{55}$$

Hypoplasticity:

$$\dot{\boldsymbol{\varepsilon}}^{hp} = Y\,\mathbf{m}\,||\dot{\boldsymbol{\varepsilon}}||, \tag{56}$$

$$Y = \left[Y_0 + (1-Y_0)\,Y_D\right]\,\mathrm{OCR}^{-n_{OCR}}, \quad Y_0 = \frac{\lambda-\kappa}{\lambda+\kappa}\left(\frac{p_{ei}}{p}\right)^2, \tag{57}$$

$$\mathbf{m} = \left(-\frac{1}{3}\sqrt{\frac{2}{3}}\,d\,\mathbf{1} + \vec{\boldsymbol{\sigma}}^{*}\right)^{\rightarrow} \tag{58}$$

Viscosity:

$$\dot{\boldsymbol{\varepsilon}}^{vis} = I_v\,\lambda\left(\frac{1}{\mathrm{OCR}}\right)^{1/I_v}\mathbf{m}, \tag{59}$$

$$\mathrm{OCR} = \frac{p_{ei}}{p_{ei}^{+}}, \quad p_{ei}^{+} = \exp\left(\frac{e_{i0}-e^{+}}{\lambda}\right) \tag{60}$$

$$e^{+} = A^{1/n_f}\,e_i, \quad A = 1 - \left(\frac{|\eta|}{M f_{b0}}\right), \quad n_f = \frac{\ln(f_{b0}^2 - 1)/f_{b0}^2}{\ln(e_c/e_i)} \tag{61}$$

References

1. Andersen, K.H.: Bearing capacity under cyclic loading - offshore, along the coast, and on land. Can. Geotech. J. **46**(5), 513–535 (2009)
2. Cattoni, E., Tamagnini, C.: On the seismic response of a propped r.c. diaphragm wall in a saturated clay. Acta Geotech. (2019). https://doi.org/10.1007/s11440-019-00771-4
3. Taylor, D.W.: Fundamentals of Soil Mechanics. Wiley, New York (1954)
4. Rowe, P., Taylor, G.I.: The stress-dilatancy relation for static equilibrium of an assembly of particles in contact. Proc. Roy. Soc. Lond. Math. Phys. Sci. **269**, 500–527 (1962)
5. Pradhan, T.B.S., Tatsuoka, F., Sato, Y.: Experimental stress-dilatancy relations of sand subjected to cyclic loading. Soils Found. **29**(1), 45–64 (1989)

6. Li, X.S., Dafalias, Y.F.: Dilatancy for cohesionless soils. Géotechnique **50**(4), 449–460 (2000)
7. Yang, Z., Xu, T.: J2-deformation type model coupled with state dependent dilatancy. Comput. Geotech. **105**, 129–141 (2019)
8. Wan, R.G., Guo, P.J.: Stress dilatancy and fabric dependence on sand behavior. J. Eng. Mech. **160**(6), 635–645 (2004)
9. Wichtmann, T.: Soil behaviour under cyclic loading - experimental observations, constitutive description and applications. Veröffentlichungen des Instituts für Bodenmechanik und Felsmechanik am KIT, Habilitation, no. 181 (2016)
10. Pradhan, T.B.S., Tatsuoka, F.: On stress-dilatancy equations of sand subjected to cyclic loading. Soils Found. **29**(1), 65–81 (1989)
11. Verdugo, R., Ishihara, K.: The steady state of sandy soils. Soils Found. **36**(2), 65–81 (1996)
12. Coop, M.R., Atkinson, J.H., Taylor, R.N.: Strength and stiffness of structured and unstructured soils. In: Proceedings of the 11th European Conference on Soil Mechanics and Foundation Engineering, Copenhagen, vol. 1, pp. 55–62 (1995)
13. Amorosi, A., Rampello, S.: An experimental investigation into the mechanical behaviour of a structured stiff clay. Géotechnique **57**(2), 153–166 (2007)
14. Wichtmann, T., Triantafyllidis, T.: Monotonic and cyclic tests on kaolin: a database for the development, calibration and verification of constitutive models for cohesive soils with focus to cyclic loading. Acta Geotech. **13**(5), 1103–1128 (2017)
15. Tafili, M., Triantafyllidis, T.: A simple hypoplastic model with loading surface accounting for viscous and fabric effects of clays. Submitted for IJNAMG (2017)
16. Matsuoka, H., Nakai, T.: A new failure for soils in three-dimensional stresses. In: Proceedings of the IUTAM Symposium on Deformation and Failure of Granular Materials, Delft, pp. 253–263 (1982)
17. Argyris, J.H., Faust, G., Szimmat, J., Warnke, E.P., Willam, K.J.: Recent developments in the finite element analysis of prestressed concrete reactor vessels. Nucl. Eng. Des. **282**(1), 42–75 (1974)
18. Taiebat, M., Dafalias, Y.F.: SANISAND: simple anisotropic sand plasticity model. Int. J. Numer. Anal. Meth. Geomech. **32**, 915–948 (2008)
19. Fuentes, W., Triantafyllidis, T.: ISA model: a constitutive model for soils with yield surface in the intergranular strain space. Int. J. Numer. Anal. Meth. Geomech. **39**(11), 1235–1254 (2015)
20. Fuentes, W., Tafili, M., Triantafyllidis, T.: An ISA-plasticity-based model for viscous and non-viscous clays. Acta Geotech. **13**(2), 367–386 (2017)
21. Pradhan, T.B.S., Tatsuoka, F., Mohri, Y., Sato, Y.: An automated triaxial testing system using a simple triaxial cell for soils. Soils Found. **29**(1), 151–160 (1989)
22. Ishihara, K., Tatsuoka, F., Yasuda, S.: Undrained deformation and liquefaction of sand under cyclic stresses. Soils Found. **15**(1), 29–44 (1975)
23. Dafalias, Y.F., Manzari, M.T.: Simple plasticity sand model accounting for fabric change effects. J. Eng. Mech. **130**(6), 622–634 (2004)
24. Grandas, C., Triantafyllidis, T.: Personal communication. Institute of Soil Mechanics and Rock Mechanics (IBF, KIT) (2019)
25. Roscoe, K.H., Schofield, A.N.: Mechanical behaviour of an idealized 'wet' clay. In: Proceedings of the European Conference on Soil Mechanics and Foundation Engineering, Wiesbaden, vol. 1, pp. 47–54 (1963)
26. Roscoe, K.H., Burland, J.B.: On the generalized stress-strain behaviour of 'wet' clay. Engineering plasticity, pp. 535–609 (1968)
27. Masin, D.: Hypoplastic models for fine-grained soils. Ph.D. thesis, Charles University, Prague (2006)

28. Niemunis, A.: Extended hypoplastic models for soils. Habilitation, Monografia 34, Ruhr-University Bochum (2003)
29. Niemunis, A., Grandas, C., Prada, L.: Anisotropic Visco-hypoplasticity. Acta Geotech. **4**(4), 293–314 (2009)
30. Finno, R.J., Chung, C.K.: Stress-strain-strength responses of compressible Chicago glacial clays. J. Geotech. Eng. ASCE **118**(10), 1607–1625 (1992)
31. Yasuhara, K., Hirao, K., Hyde, A.: Effects of cyclic loading on undrained strength and compressibility of clay. Soils Found. **32**(1), 100–116 (1992)
32. Bohac, J., Herle, I., Feda, J., Klablena, P.: Properties of fissured Brno clay. In: Proceedings of the 11th European Conference on Soil Mechanics and Foundation Engineering, Copenhagen, vol. 3, pp. 19–24 (1995)
33. Sheahan, T.C., Ladd, C.C., Germaine, J.T.: Rate dependentundrained shear behavior of saturated clay. J. Geotech. Eng. ASCE **122**(2), 99–108 (1996)
34. Burland, J.B., Rampello, S., Georgiannou, V.N., Calabresi, G.: A laboratory study of the strength of four stiff clays. Géotechnique **46**(3), 491–514 (1996)
35. Rampello, S., Callisto, L.: A study on the subsoil of the tower of Pisa based on results from standard and high-quality samples. Can. Geotech. J. **35**(6), 1074–1092 (1998)
36. Sivakumar, V., Doran, I.G., Graham, J.: Particle orientation and its influence on the mechanical behavior of isotropically consolidated reconstituted clay. Eng. Geol. **66**, 197–209 (2002)
37. Gasparre, A., Nishimura, S., Coop, M.R., Jardine, R.J.: The influence of structure on the behavior of London clay. Géotechnique **57**(1), 19–31 (2007)
38. Chu, D.B., Stewart, J.P., Boulanger, R.W., Lin, P.S.: Cyclic softening of low-plasticity clay and its effect on seismic foundation performance. J. Geotech. Geoenviron. Eng. ASCE **134**(11), 1595–1608 (2008)
39. Abdulhadi, N.O., Germaine, J.T., Whittle, A.J.: Stress-dependent behavior of saturated clay. Can. Geotech. J. **49**, 907–916 (2012)
40. Duong, N.T., Suzuki, M., Hai, N.V.: Rate and acceleration effects on residual strength of kaolin and kaolin-bentonite mixtures in ring shearing. Soils Found. **58**, 1153–1172 (2018)
41. Hvorslev, M.: Physical components of the shear strength of saturated clays. In: ASCE Research Conference, Shear Strength of Cohesive Soils, Boulder Colorado (1960)
42. Atkinson, J.: The Mechanics of Soils and Foundations. McGraw-Hill, New York (1993)
43. Shibata, T.: On the volume changes of normally-consolidated clays. In: Annuals, Disaster Prevention Research Institute, Kyoto (1963). (in Chinese)
44. Tafili, M., Triantafyllidis, T.: AVISA: anisotropic visco ISA model and its performance at cyclic loading. Submitted for Acta Geotech. (2019)
45. Tafili, M., Triantafyllidis, T.: Constitutive model for viscous clays under the ISA framework. In: Triantafyllidis, T. (ed.) Holistic Simulation of Geotechnical Installation Processes - Theoretical Results and Applications, vol. 82, pp. 324–340. Springer, Heidelberg (2017)
46. Niemunis, A., Krieg, S.: Viscous behaviour of soils under oedometric conditions. Can. Geotech. J. **33**, 159–168 (1996)
47. Fuentes, W., Hadzibeti, M., Triantafyllidis, T.: Constitutive model for clays under the ISA framework. In: Triantafyllidis, T. (ed.) Holistic Simulation of Geotechnical Installation Processes - Benchmarks and Simulations, vol. 80, pp. 115–130. Springer, Heidelberg (2015)